Organic Electronics 37 (2016) 134–140

Contents lists available at ScienceDirect

Organic Electronics

journal homepage: www.elsevier.com/locate/orgel

N-phenylindole-diketopyrrolopyrrole-containing narrow band-gap materials for dopant-free hole transporting layer of perovskite solar cell

Seolhee Jeon [a, 1], Ujwal Kumar Thakur [b, 1], Daehee Lee [a], Yin Wenping [c], Dasom Kim [c], Sunjong Lee [d], Tae Kyu Ahn [c], Hui Joon Park [b, e], Bong-Gi Kim [a, *]

[a] Department of Organic and Nano System Engineering, Konkuk University, Seoul, 143-701, Republic of Korea
[b] Division of Energy Systems Research, Ajou University, Suwon, 443-749, Republic of Korea
[c] Department of Energy Science, Sungkyunkwan University, Suwon, 440-746, Republic of Korea
[d] Korea Institute of Industrial Technology, 89 Yangdaegiro-gil, Ipjang-myeon, Seobuk-gu, Cheonan-si, Chungcheongnam-do, 31056, Republic of Korea
[e] Department of Electrical and Computer Engineering, Ajou University, Suwon, 443-749, Republic of Korea

ARTICLE INFO

Article history:
Received 16 May 2016
Received in revised form
13 June 2016
Accepted 13 June 2016

Keywords:
Perovskite solar cell
Dopant-free hole transporting material
Dipolar material
Synthesis
Recombination

ABSTRACT

Novel conjugated materials, DPIO and DPIE, having same molecular configuration of both an electron donating *N*-phenylindole and an electron accepting diketopyrrolopyrrole derivative, exhibited different aggregation behavior because of the applied side chains. When DPIO and DPIE were applied to as hole transporting materials in perovskite solar cell, DPIO showed better device performance than ones with DPIE, mostly due to the aggregation-assisted enhanced electrical property. DPIO effectively extracted hole from the perovskite layer, providing over 10% PCE of cell efficiency without any chemical doping. Incident-photon-to-electron conversion efficiency (IPCE) measurement confirmed that DPIO's strong absorption in the longer wavelength region partly contributed to the light harvesting of the solar cell device. In addition, time-resolved photoluminescence (TRPL) and transient photovoltage (TPV) studies proved that the DPIO-based device, compared to the conventional Spiro-MeOTAD-based device, has better charge extraction ability and reduced charge recombination.

© 2016 Elsevier B.V. All rights reserved.

1. Introduction

Recently, organic-inorganic hybrid perovskite solar cells have drawn much interest as a promising, cost-effective alternative to silicon-based solar cells [1–11]. The power conversion efficiency (PCE) of perovskite solar cell has improved rapidly and marked around 20% PCE, in virtue of excellent light absorption, long carrier diffusion length and charge transporting properties [12–16]. Although perovskites are efficient light harvesting materials with bipolar transport properties, recent reports suggests that hole transport layer (HTL) is necessary to effectively extract hole from the perovskite layer for solar cells with better light-to-current conversion efficiency [12,16–22]. In addition, the organic hole transporting materials should have an appropriate energy level alignment with perovskites and a good charge carrier mobility, to minimize both electrical potential loss and charge recombination.

Novel hole transporting materials (HTMs) has been synthesized and characterized to provide alternatives to spiro-MeOTAD, the most common HTM employed in perovskite solar cell. Triarylamine-based HTMs [23,24], thiophene-based HTMs containing nitrile or benzothiadiazole [25,26], triarylamin-based oligomer [27] and polymeric HTMs [12,28] are representative examples. However, most of HTMs developed up to date require chemical doping for efficient hole extraction from the perovskite film. Potential issues for doped HTMs, such as high cost, complicate fabrication and dopant-induced device degradation [29,30], would be tackled in order for us to make further advancement of perovskite solar cells. Thus, inventing dopant-free HTM for perovskite solar cell is highly desirable. Electron donor–acceptor (D–A) type conjugated small molecules with planar structures have great potential for high charge carrier mobility, because of strong intermolecular interaction. However, only a few D-A type conjugated small molecules have been synthesized to use as HTL of perovskite

* Corresponding author.
E-mail address: bgkim2015@konkuk.ac.kr (B.-G. Kim).
[1] These authors contributed equally to this work.

http://dx.doi.org/10.1016/j.orgel.2016.06.019
1566-1199/© 2016 Elsevier B.V. All rights reserved.

solar cell [25,26,31–35].

Indole and its derivatives are good candidates to be served as good hole conducting materials in optoelectronic devices, because both of a planar-fused aromatic geometry and proficient electron donating characteristics [36]. However, indole's vulnerable susceptibility to oxidation often hampered direct substitution of protons with functional groups, especially at 2- or 3-positon of carbon in five-membered ring [37]. Since five-membered aromatic/heteroaromatic rings provide reduced intra-chain steric hindrance, resulting in better planar back-bond conformation in conjugated molecules, rather than comparable six-membered rings, devising an effective way of extending π-conjugation through the five-membered ring of indole or its derivatives would be helpful to provide promising hole conducting materials. In this contribution, we synthesized novel conjugated materials, DPIO and DPIE, having same molecular configuration of both an electron donating *N*-phenylindole and an electron accepting diketopyrrolopyrrole derivative. The aggregation tendency, depending on applied side chains, was characterized by means both of UV-visible absorption spectroscopy and of 2-dimensional grazing-incidence X-ray diffraction (2D-GIXRD) after film preparation and correlated with the molecular configuration calculated by means of density functional theory (DFT). When DPIO and DPIE were adopted as hole transporting materials in perovskite solar cell, they marked 10.03% and 5.36% of PCE, respectively, without any chemical doping treatment. Furthermore, doping free DPIO as HTL improved charge extraction ability from the perovskite photoactive layer and reduced charge recombination, compared to the conventional Spiro-MeOTAD as HTL, which were confirmed by time-resolved photoluminescence (TRPL) decay and transient photo-voltage (TPV), respectively. All the *J-V* characteristics of our devices showed negligible hysteresis.

2. Experimental section

2.1. Materials

All starting materials were purchased from commercial suppliers (Aldrich and Wako Pure Chemicals). Detailed synthetic procedures are summarized as follows, and compound **3** and **4** were prepared as previously described manner [38]. Synthesized compounds were fully characterized with ^{1}H NMR and GC-mass, and elemental analysis, and the detailed synthetic procedures are illustrated in supporting information section.

2.2. Device fabrication

Devices were fabricated on fluorine-doped tin oxide (FTO) coated glass. To prevent shunting upon contact with measurement pins, FTO was etched from regions under the anode contact by etching with 35% HCL and zinc powder. Substrates were then cleaned subsequently in acetone, isopropanol, deionized water and oxygen plasma. About 50 nm of hole blocking layer of compact TiO_2 (bl-TiO_2) was deposited by spin casting twice a 0.15 M solution of titanium diisopropoxide bis(acetylacetone) (75%in 2-propanol, Sigma-Aldrich) diluted in isopropanol and annealed at 500 °C for 30 min. The substrates were treated with 0.04 mol of $TiCl_4$ (Sigma-Aldrich). Substrates were frozen in 200 ml of deionized water and then 440 μl of $TiCl_4$ was added and heated at 140 °C for an hour. About 250 nm thick mesoporous TiO_2 (mp-TiO_2) layer was then deposited over the bl-TiO_2 by spin casting a solution of commercial TiO_2 paste (Dyesol 30NRD) in anhydrous ethanol and annealed at 500 °C for 30 min. Then the substrates were subsequently cleaned with deionized water and ethanol and annealed at 500 °C for 30 min. 1 mol PbI_2 (99.9% Sigma-Aldrich) solution in DMF, stirred for 8 h at 70 °C, was then spin coated over the substrate and annealed at 70 °C for 5 min. After that, CH_3NH_3I was deposited and annealed at 110 °C for 10 min. On the top of perovskite layer, DPIO, DPIE or Spiro-MeOTAD was spin-casted as a HTL (150 nm), and Au (70 nm) was thermally deposited as an electrode, finally giving a following device configuration: FTO/bl-TiO_2/mp-TiO_2/$CH_3NH_3PbI_3$/HTL/Au.

2.3. Device characterization

Current voltage characteristics of all devices ware measured by applying external bias to the cell while recording generated photocurrent. A solar simulator (PEC-L01, Peccell Technologies, Inc.) with an AM 1.5G filter was used to provide 100 mWcm^{-2} of illumination on the PV cells, calibrated using a Si photodiode. *J-V* characteristics were obtained using an Ivium technology Ivium compactstat by scanning the *J-V* curves at a 0.05 Vs^{-1} scan rate. The incident-photon-to-electron conversion efficiency (IPCE) was measured under short-circuit conditions using ABET Technology 10,500 solar simulator as the light source and a SPECTRO Mmac-200 as the light solution. SEM images were captured by Hitachi S-4800. TRPL curves were recorded using a commercial Time-Correlated Single Photon Counting (TCSPC) system (FluoTim 200, PicoQuant) [39]. Samples were photoexcited by picosecond diode laser of 670 nm (LDH-P-C-670, PicoQuant) with a variable repetition rate (1 MHz). The emitted PL was spectrally dispersed with monochromator (ScienceTech 9030) for each PL signal, and was collected by a fast photon multiplier tube (PMT) detector (PMA 182, PicoQuant GmbH) with a magic angle (54.7°) arrangement. The incident angle of excitation pulse was set to be about 30° with respect to the sample. The resulting instrumental response function was about 160 ps in full-width-half-maximum. And all of the signals were measured at the emission peak (770 ± 5 nm) for perovskite. In addition, a cut-off filter (FF01-692 nm, Semrock) was applied to block the remaining scattering. Transient photovoltage decay measurements was performed using a nanosecond laser (pulsed 10 Hz, NT342A-10, EKSPLA) pumped OPO pulse of 550 nm and a Xe lamp (continuous wave, 150 W, Zolix) as a attenuated perturbation light pulse and a bias light source, respectively. The sample devices were electrically connected to a digital oscilloscope (500 MHz, DSO-X 3054A, Agilent) with BNC cables, and the input impedance was set to be 1 MΩ (Keithley 2001) for an open circuit condition. The bias light intensity was controlled by neutral density filters (from 0.0 to 1.0 sun) for the generation of various open circuit voltages (V_{oc}). For the photocurrent measurement of samples, the input impedance of 50 Ω termination was used instead for a closed circuit conditions without any optical setup change.

3. Results and discussions

As illustrated in Fig. 1a and Scheme S1, 3-bromo-1-phenyl-1H-indole (**1**) was selectively synthesized via a direct bromination from 1-phenyl-1H-indole, and the obtained compound **1** was kept into n-hexane at −10 °C after purification, to prevent oxidation-induced decomposition. Compound **2** obtained after introducing an electron withdrawing boronate into 1-phenyl-1H-indole showed enough stability to handle under ambient condition. Final products, DPIO and DPIE, were successfully obtained via Suzuki-type coupling between the compound **2** and DPP derivatives. To characterize aggregation tendency in thin film state, UV-visible absorption spectra of obtained DPIO and DPIE were compared both in solutions and in films (Fig. 1b). DPIO and DPIE, in diluted chloroform solution, exhibited nearly same absorption spectra having absorption maximum around 625 nm, but their absorption behaviors were different in film state. In the case of DPIO film, it exhibited similar

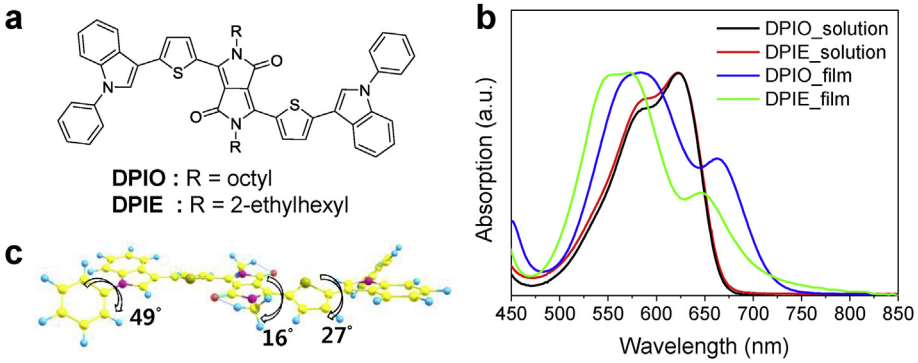

Fig. 1. (a) Chemical structures of obtained DPIO and DPIE and (b) their absorption spectra both in solution and in film states. (c) Optimized molecular configuration of DPIO and DPIE.

absorption peak around 575 nm with that of corresponding solution and resulted in more developed absorption around 665 nm when the film was thermally annealed at 125 °C for 10 min. On the other hand, the main absorption of DPIE film blue-shifted from 590 nm to 540 nm and newly developed absorption band appeared around 645 nm with relatively weak intensity, compared to that of DPIO. In general, the absorption development in longer wavelength region, compared to absorption in solution, implies molecular aggregation between π-conjugated backbones. Thus, the absorption spectra imply that DPIO has better capability to form intermolecular packing.

The strong aggregation tendency of DPIO was verified with 2D-GIXRD. As shown in Fig. S1, DPIO exhibited intense diffraction, indicating strong aggregation nature in film state. However, DPIE did not show any noticeable diffraction pattern, corresponding to amorphous-like nature. Because the inter-molecular π-orbital overlap facilitates inter-molecular carrier transfer, providing outperforming electrical properties in organic semiconductors [40,41], DPIO has great potential for electronic device applications. The origin of different aggregation characteristics between DPIO and DPIE can be traced from side-chain induced steric hindrance. Although both materials share inherently planar back-bond geometry induced by reduced intramolecular steric hindrance via chemical bonds between 5-membered aromatic rings (indole and thiophene), two bulky 2-ethylhexyl groups in one DPIE molecule could suppress the propensity of intermolecular packing effectively. To validate planar-backbone geometry, a computational pre-optimization was carried out using AM1 semi-empirical quantum chemistry model [42]. The resulting molecular configuration was then further optimized with B3LYP as the exchange-correlation functional in the density functional theory (DFT) framework. As illustrated in Fig. 1b, the torsional angle between thiophene and indole was estimated about 27° based on computational optimization, which implies that DPIO and DPIE have planar backbone configurations.

DPIO and DPIE resulted in nearly same energy levels. The optical band-gap estimated by the absorption onset of cast films was to be 1.7 eV, and the HOMO energy level measured by means of cyclic voltammetry was −4.9 eV (Fig. S2). Their shallow HOMO level, compared to that (−5.4 eV) of perovskite, would be beneficial to extract hole from perovskite layer (Fig. 2a). In addition, the shallow LUMO level (−3.2 eV) would effectively block electron transfer from perovskite layer to DPIO or DPIE layer, finally resulting in unidirectional charge carrier movement in perovskite solar cell. Based on the obtained energy levels and the tendency of intermolecular packing, we could speculate that DPIO and DPIE have enough potential to function as efficient hole transporting materials in perovskite solar cell. To investigate the performance of DPIO and DPIE as HTMs, we fabricated perovskite solar cells as following configuration: FTO/bl-TiO_2/mp-TiO_2/$CH_3NH_3PbI_3$/HTL/Au. In addition, Spiro-MeOTAD, one of the most efficient hole transporting materials in perovskite solar cells, was applied together, to relatively compare the function of DPIO and DPIE as HTL in perovskite solar cells.

First, the function of HTL in perovskite solar cell was examined by eliminating the HTL from the same architectural solar cell device. As shown Fig. 3a and Table 1, solar cell devices adopting HTL exhibited both improved current density (J_{sc}) and higher open circuit voltage (V_{oc}), compared to the corresponding device having no HTL, which suggests that the role of HTL in perovskite solar cell rapidly extracts holes and effectively prevents the wrong-way movement of spontaneously generated electrons [43]. When the function of HTM was compared between DPIO, DPIE and Spiro-MeOTAD, DPIO exhibited higher V_{oc} and better fill factor (FF) under no chemical doping treatment, and ultimately produced over 10% PCE (Fig. 3a and Table 1). In addition, IPCE measurement revealed somewhat different photon-to-current conversion behavior between DPIO, DPIE and Spiro-MeOTAD (Fig. 3b). In the case of solar cell device adopting Spiro-MeOTAD as a HTL, it exhibited nearly same photon-to-current conversion feature with the device having no HTL, only except enhanced conversion efficiency at almost overall wavelength. However, the device adopting DPIO and DPIE as HTLs showed enhanced photon-to-current conversion efficiency around 700 nm where the perovskite has weak absorption. Since DPIO and DPIE still have decent absorption intensity around 700 nm, the higher IPCE of perovskite solar cells adopting DPIO and DPIE as HTLs could be partly ascribed to the contribution of HTL's absorption, not only from the perovskite layer. Considering that the photon flux of sunlight has higher intensity in longer wavelength region, hole transporting material having a strong absorption in longer wavelength region would be expected for improved current generation in perovskite solar cells. To confirm the reliability of fabricated device in this research, we checked *J-V* characteristics of solar cells depending on scan directions (Fig. 3c, d and Fig. S3), and all devices adopting HTL showed negligible hysteresis (Table 1), indicating stable operation of the cells.

The higher FF of DPIO-based device could be ascribed to its strong aggregation tendency. The planar geometry of DPIO having linear side chains improves intermolecular packing, consequently facilitating hole transporting behavior without any support of chemical dopants. When series resistance of each perovskite solar cells adopting different hole transporting materials, the device adopting DPIO as HTL exhibited lowest value as summarized in Table 1, which could be fairly connected with the aggregation-assisted facile hole transporting property of DPIO. However, in

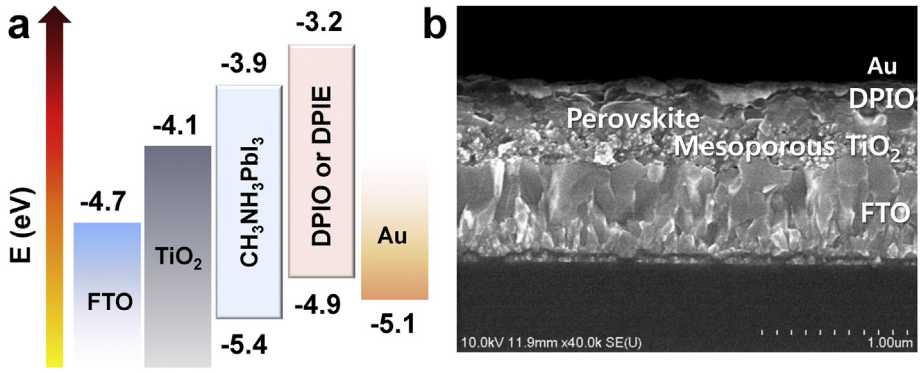

Fig. 2. (a) Relative energy level diagram of a perovskite solar cell. (b) Cross-sectional SEM image of the perovskite solar cell adopting DPIO as HTL.

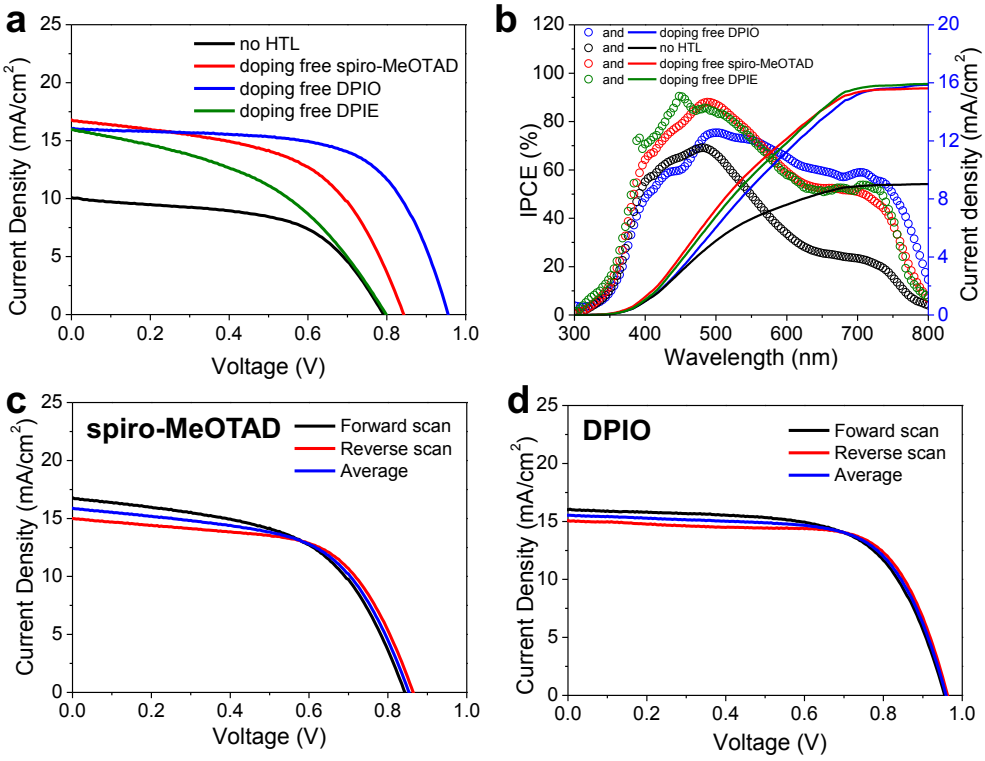

Fig. 3. (a) and (b) Device performance and IPCE of perovskite solar cell adopting different hole transporting materials. (c) and (d) Hysteresis behaviors of the fabricated solar cells.

Table 1
Summary of device performance of perovskite solar cell adopting different hole transporting materials at forward and reverse voltage scans.

HTL material	Scan direction	V_{oc} (V)	J_{sc} (mA/cm^2)	FF	PCE (%)	R_s (Ωcm^2)
N/A	Forward scan	0.79	10.10	0.56	4.46	17.1
Spiro (without Dopant)	Forward scan	0.84	16.79	0.54	7.64	10.9
	Reverse scan	0.86	14.99	0.61	7.87	10.9
	Average	0.85	15.89	0.58	7.75	10.9
DPIE	Forward scan	0.84	15.75	0.40	5.32	22.0
	Reverse scan	0.86	15.18	0.41	5.40	20.2
	Average	0.85	15.47	0.41	5.36	21.1
DPIO	Forward scan	0.96	16.00	0.65	9.92	8.3
	Reverse scan	0.96	15.08	0.70	10.14	7.6
	Average	0.96	15.54	0.67	10.03	8.0

the case of DPIE and Spiro-MeOTAD, they exhibit poor hole transporting property due to amorphous nature originated from bulky side chains and twisted molecular configuration, respectively. The amorphous characteristics of HTL cause strong hole accumulation including strong charge recombination, unless it is properly doped to improve electrical property [44,45]. When Spiro-MeOTAD was doped with Li-TFSI and 4-*tert*-butylpryidine, the device performance was dramatically enhanced with the PCE of 11.84%, combined with a J_{sc} of 17.41 mA/cm^2, an V_{oc} of 0.99 V, and FF of 69%, mainly due to the improved electrical conductivity (Fig. S4). We applied the dopants to DPIO and DPIE, respectively but could not see the enhancement of devices performance under the same doping system with the Spiro-MeOTAD. Although the doped Sprio-MeOTAD exhibited slightly better device performance than DPIO, the dopant free system is still competitive, because of simple fabrication, cost effectiveness and freedom from dopant-induced device degradation [16,29,30].

In spite of shallow HOMO level rather than that of Spiro-MeOTAD, the DPIO-based device showed higher V_{oc}. We think that this would be mostly due to the reduced charge recombination, originated from both the aggregation-induced enhanced electrical property and the strong molecular dipole created by the DPP moiety. The enhanced FF reflects a thread of connection with the suppressed charge recombination in DPIO-based perovskite solar cell. To examine the improved charge extraction ability of doping free DPIO, TRPL decay of Quartz(Q)/$MAPbI_3$/doping free Spiro-MeOTAD and Q/$MAPbI_3$/doping free DPIO was carried out keeping Q/$MAPbI_3$ as the reference. The PL decay curves of each samples were convoluted using multiple exponential functions and are plotted in Fig. 4a. According to bi-exponential fitting, the Q/$MAPbI_3$ showed a medium component of about 5.77 ns and a long component 17.80 ns (Table S1), which should be originated from bimolecular recombination in perovskite active layer and free carriers recombination in the radiative channel, respectively [46,47]. This result also show good consistency with documented lectures [48,49]. However, for samples with HTL (Spiro-MeOTAD and DPIO), new sub-nanosecond fast component (0.54 ns and 0.27 ns) was found by a result of tri-exponential fitting, Q/MAPbI3/DPIO even showed larger weight ratio (71.44%) for that component. Although that minority picosecond fast component is normally covered by medium lifetime in TRPL [50], we specially compared signals for the same samples excited from both of back (Q) side and front (HTL) side (Fig. S5 and Table S2), which revealed clear new content for front side measurement. All those indicate the new fast component should come from the interface process between perovskite and HTL, while that effect gets decreased when we measure from back side due to the finite carrier diffusion length. The rate of charge separation (K_{cs}) for Quartz(Q)/$MAPbI_3$/Spiro-MeOTAD and Q/$MAPbI_3$/DPIO were calculated to be 1.76 × 109 s^{-1} and 3.62 × 109 s^{-1}, respectively. All of higher weight ratio and faster charge separation rate demonstrate that DPIO showed more than two times of charge extraction ability compare to Spiro-MeOTAD, which results in the higher PCE for $MAPbI_3$/DPIO device. To compare the charge recombination lifetime of the device with doping free DPIO, we examined the TPV for devices having doping free Spiro-MeOTAD and doping free DPIO as HTL, and without HTL as a reference. Fig. 4b shows the averaged charge recombination lifetimes (τ_n) from three devices with increment in open circuit voltage. Generally, the device with longer charge recombination time has better efficiency as the longer recombination time will increase the possibility of charge extraction. Device with doping free DPIO as HTL revealed higher charge recombination times than that of device with doping free Spiro-MeOTAD as HTL in the entire range of open circuit voltage. It also indicates clearly that the trap density for device with DPIO may be lower than that for device with Spiro-MeOTAD. It may be due to larger carrier mobility in DPIO. Overall, it could be concluded that the device with DPIO will have better dynamics compared to the devices with Spiro-MeOTAD under non-doping system.

4. Conclusions

In summary, a novel hole transporting material, DPIO and DPIE, were directly synthesized through regio-selective modification of 1-phenyl indole. The obtained DPIO showed strong aggregation tendency in film but DPIE exhibited amorphous-like nature. The aggregation behavior was characterized by means of UV-visible spectroscopy and 2D GIXRD, and the strong aggregation behavior of DPIO could be from both planar backbone geometry and linear side chains having small steric hindrance. When DPIO served as HTL in perovskite solar cell, it effectively extracted hole from the perovskite layer, providing over 10% PCE without any chemical doping. In addition, it was confirmed, by means of IPCE measurement, that DPIO's strong absorption in longer wavelength region partly contributed to the light harvesting of the solar cell device. Moreover improved charge extraction ability and reduced charge recombination in DPIO-based device, compared to the conventional Spiro-MeOTAD-based device, were proven by TRPL and TPV experiments, respectively. We believe that our result suggests solid ideas on material design strategies for high performing dopant-free HTLs in perovskite solar cell.

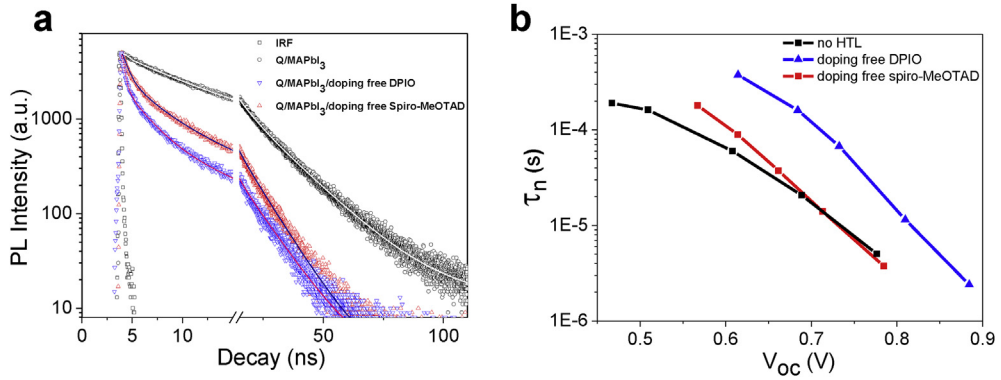

Fig. 4. (a) Time Resolved Photoluminescence (TRPL) spectra of $MAPbI_3$ (180 nm) perovskite photoactive layer on quartz substrate without hole transfer material (HTL) (black) and with HTL, doping free spiro-MeOTAD (red) and DPIO (blue), taken at peak emission wavelength (770 nm), excited at 670 nm (1 MHz) from HTL side. Symbols are measurement results and solid lines are multiple exponential fits. (b) recombination times estimated from transient photovoltage (TPV) decays with an increase of open circuit voltages (V_{oc}).

Acknowledgment

This research was supported by Basic Science Research Program through the National Research Foundation of Korea (NRF) funded by the Ministry of Science, ICT & Future Planning (NRF-2015R1C1A1A02036659) and the Ministry of Education (NRF-2014R1A1A2056403). This research was also supported by the Ministry of Trade, Industry & Energy (MOTIE, 10051565) and KDRC (Korea Display Research Corporation) support program for the development of future devices technology for display industry.

Appendix A. Supplementary data

Supplementary data related to this article can be found at http://dx.doi.org/10.1016/j.orgel.2016.06.019.

References

[1] C.C. Stoumpos, C.D. alliakas, M.G. Matzidis, Semiconducting tin and lead iodide perovskites with organic cations: phase transitions, high mobilities, and near-infrared photoluminescent properties, Inorg. Chem. 52 (2013) 9019.
[2] H.S. Kim, C.R. Lee, J.H. Im, K.B. Lee, T. Moehl, A. Marchioro, S.J. Moon, R. Humphry-Baker, J.H. Yum, J.E. Moser, M. Grätzel, N.G. Park, Lead iodide perovskite sensitized all-solid-state submicron thin film mesoscopic solar cell with efficiency exceeding 9%, Sci. Rep. 2 (2012) 591.
[3] M.A. Green, A. Ho-Baillie, H.J. Snaith, The emergence of perovskite solar cells, Nat. Photonics 8 (2014) 506.
[4] A. Kojima, K. Teshima, Y. Shirai, T. Miyasaka, Organometal halide perovskites as visible-light sensitizers for photovoltaic cells, J. Am. Chem. Soc. 131 (2009) 6050–6051.
[5] M. Grätzel, The light and shade of perovskite solar cells, Nat. Mater. 13 (2014) 838–842.
[6] J. Burschka, N. Pellet, S.J. Moon, R. Humphry-Baker, P. Gao, M.K. Nazeeruddin, M. Grätzel, Sequential deposition as a route to high-performance perovskite-sensitized solar cells, Nature 499 (2013) 316–319.
[7] Q. Chen, H.P. Zhou, Z.R. Hong, S. Luo, H.S. Duan, H.H. Wang, Y.S. Liu, G. Li, Y. Yang, Planar heterojunction perovskite solar cells via vapor-assisted solution process, J. Am. Chem. Soc. 136 (2014) 622–625.
[8] M.M. Lee, J. Teuscher, T. Miyasaka, T.N. Murakami, H.J. Snaith, Efficient hybrid solar cells based on meso-superstructured organometal halide perovskites, Science 338 (2012) 643–647.
[9] M.Z. Liu, M.B. Johnston, H.J. Snaith, Efficient planar heterojunction perovskite solar cells, Nature 501 (2013) 395–398.
[10] N.J. Jeon, H.G. Lee, Y.C. Kim, J. Seo, J.H. Noh, J. Lee, S.I. Seok, o-Methoxy substituents in spiro-OMeTAD for efficient inorganic–organic hybrid perovskite solar cells, J. Am. Chem. Soc. 136 (2014) 7837–7840.
[11] N.J. Jeon, J.H. Noh, Y.C. Kim, W.S. Yang, S. Ryu, S.I. Seok, Solvent engineering for high-performance inorganic-organic hybrid perovskite solar cells, Nat. Mater. 13 (2014) 897–903.
[12] N.J. Jeon, J.H. Noh, W.S. Yang, Y.C. Kim, S. Ryu, J. Seo, S.I. Seok, Compositional engineering of perovskite materials for high-performance solar cells, Nature 517 (2015) 476–480.
[13] W. Nie, H. Tsai, R. Asadpour, J.-C. Blancon, A.J. Neukirch, G. Gupta, J.J. Crochet, M. Chhowalla, S. Tretiak, M.A. Alam, H.-L. Wang, A.D. Mohite, High-efficiency solution-processed perovskite solar cells with millimeter-scale grains, Science 347 (2015) 522–525.
[14] W.S. Yang, J.H. Noh, N.J. Jeon, Y.C. Kim, S. Ryu, J. Seo, S.I. Seok, High-performance photovoltaic perovskite layers fabricated through intramolecular exchange, Science 348 (2015) 1234–1237.
[15] C.-G. Wu, C.-H. Chiang, Z.-L. Tseng, M.K. Nazeeruddin, A. Hagfeldt, M. Grätzel, High efficiency stable inverted perovskite solar cells without current hysteresis, Energy Environ. 8 (2015) 2725–2733.
[16] H. Zhou, Q. Chen, G. Li, S. Luo, T. Song, H.-S. Duan, Z. Hong, J. You, Y. Liu, Y. Yang, Interface engineering of highly efficient perovskite solar cells, Science 345 (2014) 542–546.
[17] J.W. Lee, D.J. Seo, A.N. Cho, N.G. Park, High-efficiency perovskite solar cells based in the black polymorph of $HC(NH_2)_2PbI_3$, Adv. Mater. 26 (2014) 4991–4998.
[18] J.A. Christians, R.C.M. Rung, P.V. Kamat, An inorganic hole conductor for organo-lead halide perovskite solar cells. Improved hole conductivity with copper iodide, J. Am. Chem. Soc. 136 (2014) 758–764.
[19] B. Conings, L. Baeten, C.D. Dobbelaere, J. D'Haen, J. Manca, H.G. Boyen, Perovskite-based hybrid solar cells exceeding 10% efficiency with high reproducibility using a thin film sandwich approach, Adv. Mater. 26 (2014) 2041–2046.
[20] Y.S. Kwon, J. Lim, H.J. Yun, Y.H. Kim, T. Park, A diketopyrrolopyrrole-containing hole transporting conjugated polymer for use in efficient stable organic–inorganic hybrid solar cells based on a perovskite, Energy Environ. Sci. 7 (2014) 1454–1460.
[21] O. Malinkiewicz, A. Yella, Y.H. Lee, G.M. Espallargas, M. Graetzel, M.K. Nazeeruddin, H.J. Bolink, Perovskite solar cells employing organic charge-transport layers, Nat. Photonics 8 (2014) 128–132.
[22] Z. Hawash, L.K. Ono, S.R. Raga, M.V. Lee, Y.B. Qi, Air-exposure induced dopant redistribution and energy level shifts in spin-coated spiro-MeOTAD films, Chem. Mater. 27 (2015) 562–569.
[23] N.J. Jeon, J. Lee, J.H. Noh, M.K. Nazeeruddin, M. Grätzel, S.I. Seok, Efficient inorganic–organic hybrid perovskite solar cells based on pyrene arylamine derivatives as hole-transporting materials, J. Am. Chem. Soc. 135 (2013) 19087.
[24] H. Li, K. Fu, A. Hagfeldt, M. Grätzel, S.G. Mhaisalkar, A.C. Grimsdale, A simple 3,4-ethylenedioxythiophene based hole-transporting material for perovskite solar cells, Angew. Chem. Int. Ed. 53 (2014) 4085.
[25] P. Qin, H. Kast, M.K. Nazeeruddin, S.M. Zakeeruddin, A. Mishra, P. Bäuerle, M. Grätzel, Low band gap S,N-heteroacene-based oligothiophenes as hole-transporting and light absorbing materials for efficient perovskite-based solar cells, Energy Environ. Sci. 7 (2014) 2981.
[26] P. Qin, S. Paek, M.I. Dar, J. Ko, M. Grätzel, M.K. Nazeeruddin, Perovskite solar cells with 12.8% efficiency by using conjugated quinolizino acridine based hole transporting material, J. Am. Chem. Soc. 136 (2014) 8516.
[27] P. Qin, N. Tetreault, M.I. Dar, P. Gao, K.L. McCall, S.R. Rutter, S.D. Ogier, N.D. Forrest, J.S. Bissett, M.J. Simms, A.J. Page, R. Fisher, M. Grätzel, M.K. Nazeeruddin, Stable and efficient perovskite solar cells based on titania nanotube arrays, Adv. Energy Mater. (2014) 1400980.
[28] Y.S. Kwon, J. Lim, H.J. Yun, Y.H. Kim, T. Park, A diketopyrrolopyrrole-containing hole transporting conjugated polymer for use in efficient stable organic–inorganic hybrid solar cells based on a perovskite, Energy Environ. Sci. 7 (2014) 1454–1460.
[29] G.E. Eperon, V.M. Burlakov, P. Docampo, A. Goriely, H.J. Snaith, Morphological control for high performance, solution-processed planar heterojunction perovskite solar cells, Adv. Funct. Mater. 24 (2014) 151.
[30] J. Liu, Y.Z. Wu, C.J. Qin, X.D. Yang, T. Yasuda, A. Islam, K. Zhang, W.Q. Peng, W. Chen, L.Y. Han, A dopant-free hole-transporting material for efficient and stable perovskite solar cells, Energy Environ. Sci. 7 (2014) 2963.
[31] G.-W. Kim, G. Kang, J. Kim, G.-Y. Lee, H.-I. Kim, L. Pyeon, J. Lee, T. Park, Dopant-free polymeric hole transport materials for highly efficient and stable perovskite solar cells, Energy Environ. Sci. (2016), http://dx.doi.org/10.1039/C6EE00709K.
[32] Y. Liu, Q. Chen, H.-S. Duan, H. Zhou, Y. Yang, H. Chen, S. Luo, T.-B. Song, L. Dou, Z. Hong, Y. Yang, A dopant-free organic hole transport material for efficient planar heterojunction perovskite solar cells, J. Mater. Chem. A 3 (2015) 11940–11947.
[33] M. Franckevičius, A. Mishra, F. Kreuzer, J. Luo, S.M. Zakeeruddin, M. Grätzel, A dopant-free spirobi[cyclopenta[2,1-b:3,4-b′]dithiophene] based hole-transport material for efficient perovskite solar cells, Mater. Horiz. 2 (2015) 613–618.
[34] W. Chen, X. Bao, Q. Zhu, D. Zhu, M. Qiu, M. Sun, R. Yang, Simple planar perovskite solar cells with a dopant-free benzodithiophene conjugated polymer as hole transporting material, J. Mater. Chem. C 3 (2015) 10070–10073.
[35] G. Gong, N. Zhao, D. Ni, J. Chen, Y. Shen, M. Wang, G. Tu, Dopant-free 3,3′-bithiophene derivatives as hole transport materials for perovskite solar cells, J. Mater. Chem. A 4 (2016) 3661–3666.
[36] G.D. Sharma, M.A. Reddy, K. Ganesh, S.P. Singh, M. Chandrasekharam, Indole and triisopropyl phenyl as capping units for a diketopyrrolopyrrole (DPP) acceptor central unit: an efficient d–a–d type small molecule for organic solar cells, RSC Adv. 4 (2014) 732–742.
[37] S.G. Newman, M. Lautens, The role of reversible oxidative addition in selective palladium(0)-catalyzed intramolecular cross-couplings of polyhalogenated substrates: synthesis of brominated indoles, J. Am. Chem. Soc. 132 (2010) 11416–11417.
[38] H.-C. Liao, C.-H. Lee, Y.-C. Ho, M.-H. Jao, C.-M. Tsai, C.-M. Chuang, J.-J. Shyue, Y.-F. Chen, W.-F. Su, Diketopyrrolopyrrole-based oligomer modified TiO_2 nanorods for air-stable and all solution processed poly(3-hexylthiophene): TiO_2 bulk heterojunction inverted solar cell, J. Mater. Chem. 22 (2012) 10589.
[39] K.S. Sarkisyan, A.S. Goryashchenko, P.V. Lidsky, D.A. Gorbachev, N.G. Bozhanova, A.Y. Gorokhovatsky, A.R. Pereverzeva, A.P. Ryumina, V.V. Zherdeva, A.P. Savitsky, K.M. Solntsev, A.S. Bommarius, G.V. Sharonov, J.R. Lindquist, M. Drobizhev, T.E. Hughes, A. Rebane, K.A. Lukyanov, A.S. Mishin, Green fluorescent protein with anionic tryptophan-based chromophore and long fluorescence lifetime, Biophys. J. 109 (2015) 380.
[40] B.-G. Kim, E.J. Jeong, H.J. Park, D. Bilby, L.J. Guo, J. Kim, Effect of polymer aggregation on the open circuit voltage in organic photovoltaic cells: aggregation-induced conjugated polymer gel and its application for preventing open circuit voltage drop, ACS Appl. Mater. Interfaces 3 (2011) 674–680.
[41] B.-G. Kim, E.J. Jeong, J.W. Chung, S. Seo, B. Koo, J. Kim, Molecular design principle of lyotropic liquid-crystalline conjugated polymers with directed alignment capability for plastic electronics, Nat. Mater. 12 (2013) 659–664.
[42] J.J.P. Stewart, Optimization of parameters for semiempirical methods I. Method, J. Comput. Chem. 10 (1989) 209–220.
[43] M.-F. Lo, Z.-Q. Guan, T.-W. Ng, C.-Y. Chan, C.-S. Lee, Electronic structures and photoconversion mechanism in perovskite/fullerene heterojunctions, Adv. Funct. Mater. 25 (2015) 1213–1218.
[44] J. Burschka, A. Dualeh, F. Kessler, E. Baranoff, N.L. Cevey-Ha, C.Y. Yi,

M.K. Nazeeruddin, M. Gratzel, Tris(2-(1H-pyrazol-1-yl)pyridine)cobalt(III) as p-type dopant for organic semiconductors and its application in highly efficient solid-state dye-sensitized solar cells, J. Am. Chem. Soc. 133 (2011) 18042–18045.

[45] T. Leijtens, I.K. Ding, T. Giovenzana, J.T. Bloking, M.D. McGehee, A. Sellinger, Hole transport materials with low glass transition temperatures and high solubility for application in solid-state dye-sensitized solar cells, ACS Nano 6 (2012) 1455–1462.

[46] O. Gunawan, T.K. Todorov, D.B. Mitzi, Loss mechanisms in hydrazine-processed $Cu_2ZnSn(Se,S)_4$ solar cells, Appl. Phys. Lett. 97 (2010) 233506.

[47] Q. Chen, H. Zhou, T.B. Song, S. Luo, Z. Hong, H.S. Duan, L. Dou, Y. Liu, Y. Yang, Controllable Self-induced passivation of hybrid lead iodide perovskites toward high performance solar cells, Nano Lett. 14 (2014) 4158–4163.

[48] J. Yin, J. Cao, X. He, S. Yuan, S. Sun, J. Li, N. Zheng, L. Lin, Improved stability of perovskite solar cells in ambient air by controlling the mesoporous layer, J. Mater. Chem. A 3 (2015) 16860–16866.

[49] J.H. Heo, M.S. You, M.H. Chang, W. Yin, T.K. Ahn, S.J. Lee, S.J. Sung, D.H. Kim, S.H. Im, Hysteresis-less mesoscopic $CH_3NH_3PbI_3$ perovskite hybrid solar cells by introduction of Li-treated TiO_2 electrode, Nano Energy 15 (2015) 530–539.

[50] G. Xing, N. Mathews, S. Sun, S.S. Lim, Y.M. Lam, M. Grätzel, S. Mhaisalkar, T.C. Sum, Long-range balanced electron- and hole-transport lengths in organic-inorganic $CH_3NH_3PbI_3$, Science 342 (2013) 344–347.